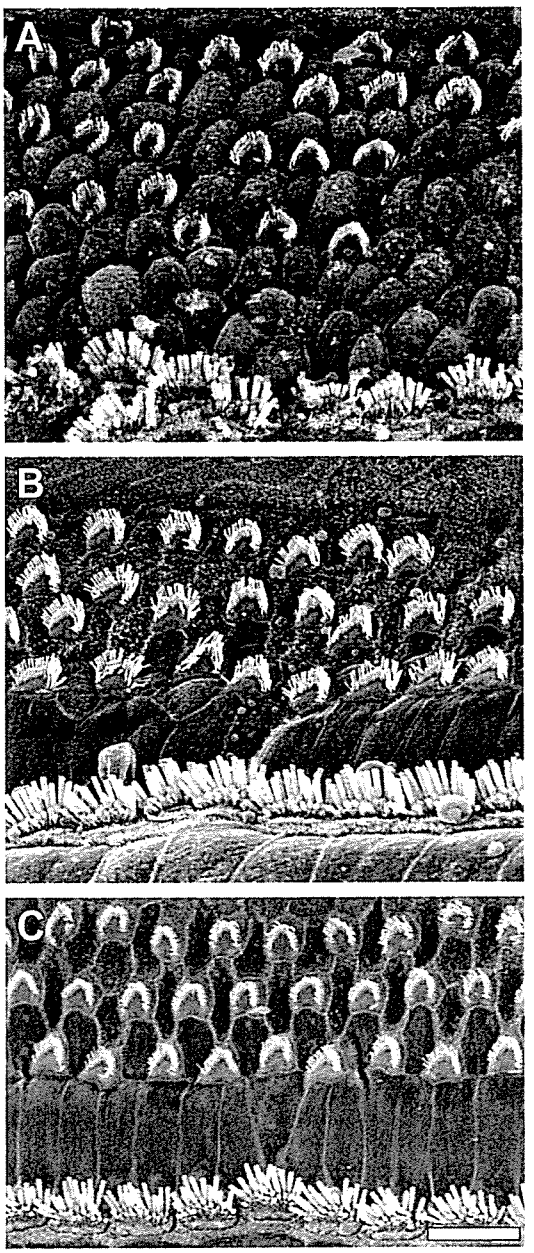

Fig. 4. SEM micrographs of the surface of the auditory epithelium in $p27^{-/-}$ (A), $p27^{+/-}$ (B) and $p27^{+/+}$ (C) mice. A: Inner hair cells are not well organized and a few of them form a second row. Outer hair cells are poorly organized and four rows can be discerned. The surface of supporting cells between outer hair cells is wider than usual and the cell borders are abnormal. The surface of the pillar cells has many more cells than in normal ears and lacks clear organization. B: The appearance of hair cells and supporting cells is close to normal. The number of cell rows is normal in both inner and outer hair cells. Pillar cell organization is slightly imperfect. C: The morphology of hair cells and supporting cells is normal. Magnification bar: 10 μm.

membrane. These nuclei appear to be attached to the basal lamina and flatten against it (Fig. 6A).

ABR audiometry (Fig. 7) shows that homozygous $p27^{-/-}$ mice have severe hearing loss at the three tested frequencies (4, 10 and 20 kHz) whereas heterozygous mice are much closer to wild-type, which exhibit normal hearing. ANOVA indicates that there are statistical differences in ABR thresholds among genotypes at each frequency. *T*-tests indicate that homozygous mutants have significantly higher thresholds than heterozygotes at each frequency. Although heterozygotes tend to have higher thresholds than wild-types, the differences were not significant at any of the tested frequencies.

4. Discussion

Overall, the structure and function of the inner ears of mice described in this report are similar to previous reports of different p27 mutations. We found that auditory function is severely impaired in $p27^{-/-}$ mice, and appears to be slightly impaired in the heterozygotes. The morphology of the sensory epithelium is consistent with the functional data and follows a similar hierarchy of pathology. Hair cells were present in all three genotypes and the most prominent pathology appeared to be in the number and organization of supporting cells.

The functional deficit in the $p27^{-/-}$ mice may be related to more than one pathology. The irregular organization of the outer hair cell area is incompatible with a normal "active" cochlea. As such, a threshold shift of 50–60 dB is expected due to the outer hair cell pathology (Dallos and Harris, 1978). In addition, it is likely that differentiation of the inner hair cells is incomplete due to crowding. Because the mosaic organization of the organ of Corti is dependent on both cell types, it is difficult to determine which cell is responsible for the primary pathology. Furthermore, p27 has a role in normal differentiation of neuronal tissues (Baldassarre et al., 2000; Sasaki et al., 2000), so the innervation of the auditory hair cells in p27 deficient mice also is likely to be abnormal.

The data obtained from cross sections of the $p27^{-/-}$ organ of Corti suggest that the excess in cell number is more prominent in supporting cells. The observation that some supporting cell nuclei are positioned flat against the basilar membrane indicates that these cells may be in s-phase, as previously shown in the regenerating auditory epithelium of birds (Raphael et al., 1994a). This suggests that new cells are still being added to the epithelium in these 21-day-old mice, more than four weeks after mitosis in the sensory epithelium is normally completed. It is possible that some of these newly-added cells differentiate into new hair cells.

Mice homozygous for the other p27 mutation (Nakayama et al., 1996) are also severely hearing impaired (Lowenheim et al., 1999), yet the pathology is not identical to that in the mouse we now describe. The organ of Corti of both p27 mutants is disorganized and includes supernumerary supporting cells and hair cells. The pathology and hearing impairment are severe in homozygotes of both mutants, but the heterozygotes seem to be slightly different. Elevated thresholds are seen in the heterozygotes of the partially deleted gene (hypomorphic mutation reported

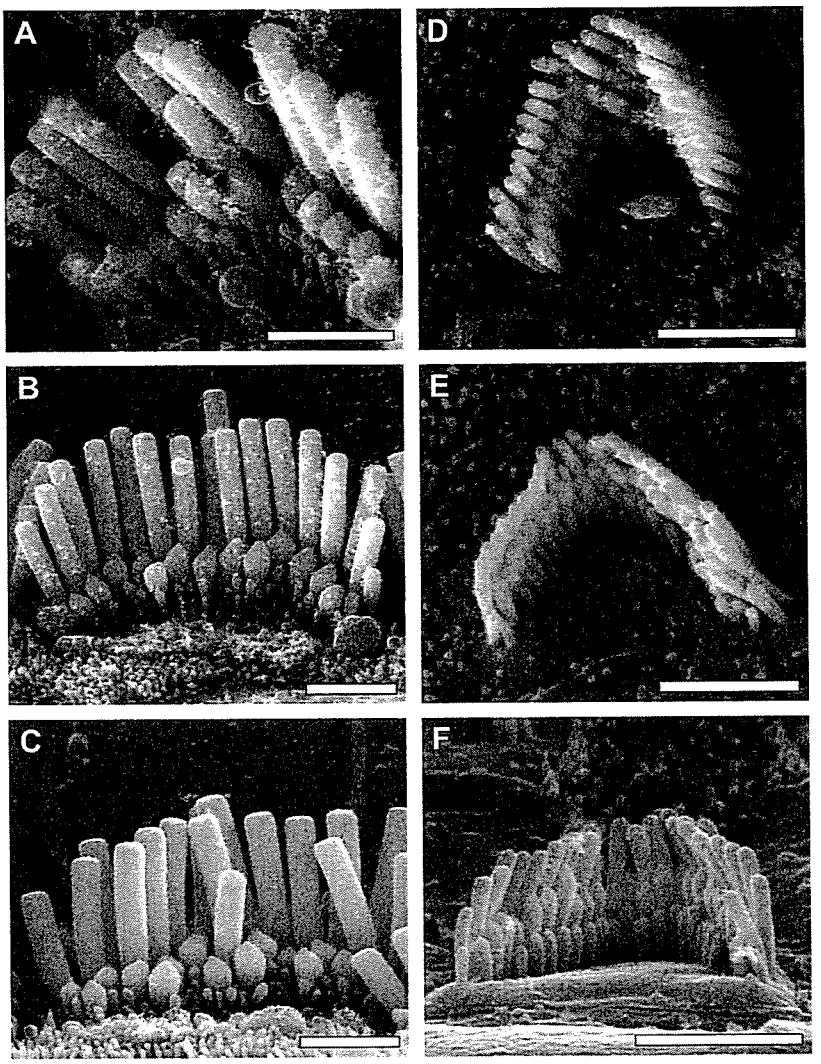

Fig. 5. SEM of apical surface of inner hair cells (A–C) and outer hair cells (D–F) of $p27^{-/-}$ (A and D), $p27^{+/-}$ (B and E) and $p27^{+/+}$ mice (C and F). The number, height and organization of stereocilia are similar in all three genotypes, but $p27^{-/-}$ hair cells appear to have slightly disorganized stereocilia, especially on the inner hair cell. Scale bars: 2 μm.

here) but not in the heterozygotes of the completely deleted p27 gene (Lowenheim et al., 1999). We speculate that the slight hearing loss in the heterozygotes of the hypomorphic deletion (studied here) is due to a dominant negative role assumed by the truncated protein in the organ of Corti. Reduced compensatory role of other genes may also play a role in the pathology seen in the hypomorphic deletion. Another possibility is that the genetic background of these hybrid mice plays a role in the severity of the heterozygote phenotype.

The genetic background of the $p27^{Kip1}$ mutant animals used in this study was hybrid 129SvJ with C57Bl/6. Both strains carry a synonymous single-nucleotide polymorphism (SNP) in exon 7 of *Cdh23* that is significantly associated with *Ahl* (Noben-Trauth et al., 2003). However, mice used in this study were 21 days old, much younger than the expected onset of age-related hearing loss, thus the pathology they exhibit is likely independent of *Ahl*.

Although the unregulated production of cells in the organ of Corti appears to involve a functional deficit, the results do have implications for designing controlled methods for inducing hair cell regeneration in the mammalian cochlea. A better understanding of cell cycle regulation in the organ of Corti may lead to enhanced ability to manipulate the genes involved in this process. Regulated inhibition of p27, Rb1 (Sage et al., 2005) or other cell cycle proteins may produce a pulse of cell generation that can be used for reconstructing the pathological organ of Corti. Skp2, a F-box protein that can inhibit p27 by unbiquitination, is present in the inner ear (Dong et al., 2003) and may be used to regulate the levels of p27. To accomplish functionally meaningful hair cell regeneration, it may also be necessary to combine the manipulation of cell cycle with induction of hair cell differentiation by genes such as *Atoh1* (Bermingham et al., 1999; Izumikawa et al., 2005; Shou et al., 2003).

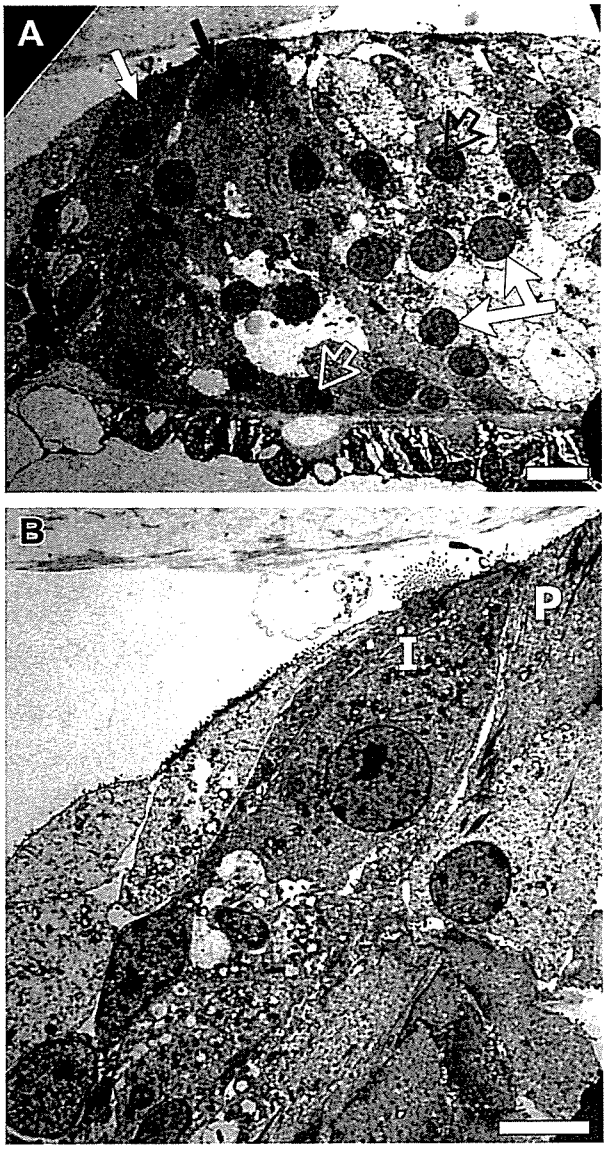

Fig. 6. TEM micrographs of organ of Corti sections in $p27^{-/-}$ cochleae. A: The inner hair cell (white filled arrow) has relatively normal morphology. Outer hair cells nuclei are present (black open arrow) but the cells bodies are pathological. Pillar cell (black filled arrow) morphology in the apical domain is abnormal, and the basal domain is not clearly identified. Supporting cell nuclei appear under the outer hair cells (double arrow) and in additional locations, including close proximity to the basilar membrane. One nucleus is flattened against the basal lamina (white open arrow). B: An inner hair cell (I) with relatively normal morphology. The adjacent pillar cell (P) appears undifferentiated and lacks typical pillar shape and cytoskeletal components. Scale bars: 10 μm in A and 5 μm in B.

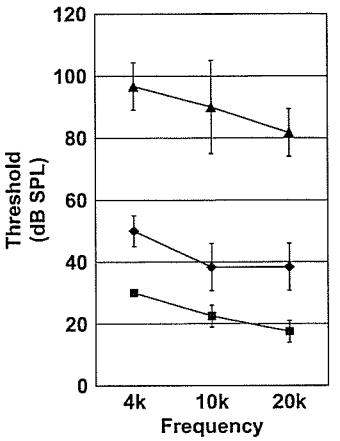

Fig. 7. ABR thresholds for the three genotypes in each of the three tested frequencies. Data points represent the mean thresholds and standard deviation. Squares are for $p27^{+/+}$, diamonds represent $p27^{+/-}$ and triangles for $p27^{-/-}$.

References

Assoian, R.K., 2004. Stopping and going with p27kip1. Dev Cell 6, 458–459.

Baldassarre, G., Boccia, A., Bruni, P., Sandomenico, C., Barone, M.V., Pepe, S., Angrisano, T., Belletti, B., Motti, M.L., Fusco, A., Viglietto, G., 2000. Retinoic acid induces neuronal differentiation of embryonal carcinoma cells by reducing proteasome-dependent proteolysis of the cyclin-dependent inhibitor p27. Cell Growth Differ. 11, 517–526.

Bermingham, N.A., Hassan, B.A., Price, S.D., Vollrath, M.A., Ben-Arie, N., Eatock, R.A., Bellen, H.J., Lysakowski, A., Zoghbi, H.Y., 1999. Math1: an essential gene for the generation of inner ear hair cells. Science 284, 1837–1841.

Chen, P., Segil, N., 1999. p27(Kip1) links cell proliferation to morphogenesis in the developing organ of Corti. Development 126, 1581–1590.

Chen, P., Zindy, F., Abdala, C., Liu, F., Li, X., Roussel, M.F., Segil, N., 2003. Progressive hearing loss in mice lacking the cyclin-dependent kinase inhibitor Ink4d. Nat. Cell Biol. 5, 422–426.

Dallos, P., Harris, D., 1978. Properties of auditory nerve responses in absence of outer hair cells. J. Neurophysiol. 41, 365–383.

Dong, Y., Nakagawa, T., Endo, T., Kim, T.S., Iguchi, F., Yamamoto, N., Naito, Y., Ito, J., 2003. Role of the F-box protein Skp2 in cell proliferation in the developing auditory system in mice. Neuroreport 14, 759–761.

Fero, M.L., Rivkin, M., Tasch, M., Porter, P., Carow, C.E., Firpo, E., Polyak, K., Tsai, L.H., Broudy, V., Perlmutter, R.M., Kaushansky, K., Roberts, J.M., 1996. A syndrome of multiorgan hyperplasia with features of gigantism, tumorigenesis, and female sterility in p27(Kip1)-deficient mice. Cell 85, 733–744.

Izumikawa, M., Minoda, R., Kawamoto, K., Abrashkin, K.A., Swiderski, D.L., Dolan, D.F., Brough, D.E., Raphael, Y., 2005. Auditory hair cell replacement and hearing improvement by Atoh1 gene therapy in deaf mammals. Nat. Med. 11, 271–276.

Kiyokawa, H., Kineman, R.D., Manova-Todorova, K.O., Soares, V.C., Hoffman, E.S., Ono, M., Khanam, D., Hayday, A.C., Frohman, L.A., Koff, A., 1996. Enhanced growth of mice lacking the cyclin-dependent kinase inhibitor function of p27(Kip1). Cell 85, 721–732.

Koff, A., Polyak, K., 1995. p27KIP1, an inhibitor of cyclin-dependent kinases. Prog. Cell Cycle Res. 1, 141–147 [Review] [37 refs].

Lowenheim, H., Furness, D.N., Kil, J., Zinn, C., Gultig, K., Fero, M.L., Frost, D., Gummer, A.W., Roberts, J.M., Rubel, E.W., Hackney, C.M., Zenner, H.P., 1999. Gene disruption of p27(Kip1) allows cell proliferation in the postnatal and adult organ of corti. Proc. Natl. Acad. Sci. USA 96, 4084–4088.

Acknowledgements

We thank Graham Atkin for technical assistance. This work was supported by Berte and Alan Hirschfield, the CHD, GM and the UAW, a grant from the Japan Ministry of Health and Labor H16-008, and NIH NIDCD Grants R01-DC05053 and R01-DC01634 and P30 DC05188.

Lumpkin, E.A., Collisson, T., Parab, P., Omer-Abdalla, A., Haeberle, H., Chen, P., Doetzlhofer, A., White, P., Groves, A., Segil, N., Johnson, J.E., 2003. Math1-driven GFP expression in the developing nervous system of transgenic mice. Gene Expr. Patterns 3, 389–395.

Nakayama, K., Ishida, N., Shirane, M., Inomata, A., Inoue, T., Shishido, N., Horii, I., Loh, D.Y., Nakayama, K., 1996. Mice lacking p27(Kip1) display increased body size, multiple organ hyperplasia, retinal dysplasia, and pituitary tumors. Cell 85, 707–720.

Noben-Trauth, K., Zheng, Q.Y., Johnson, K.R., 2003. Association of cadherin 23 with polygenic inheritance and genetic modification of sensorineural hearing loss. Nat. Genet. 35, 21–23.

Raphael, Y., 1993. Reorganization of the chick basilar papilla after acoustic trauma. J. Comp. Neurol. 330, 521–532.

Raphael, Y., Adler, H.J., Wang, Y., Finger, P.A., 1994a. Cell cycle of transdifferentiating supporting cells in the basilar papilla. Hear. Res. 80, 53–63.

Raphael, Y., Athey, B.D., Wang, Y., Lee, M.K., Altschuler, R.A., 1994b. F-actin, tubulin and spectrin in the organ of Corti: comparative distribution in different cell types and mammalian species. Hear. Res. 76, 173–187.

Ruben, R.J., 1967. Development of the inner ear of the mouse: a radio-autographic study of terminal mitoses. Acta Otolaryngol. (Suppl.), 1–44.

Sage, C., Huang, M., Karimi, K., Gutierrez, G., Vollrath, M.A., Zhang, D.S., Garcia-Anoveros, J., Hinds, P.W., Corwin, J.T., Corey, D.P., Chen, Z.Y., 2005. Proliferation of functional hair cells in vivo in the absence of the retinoblastoma protein. Science 307, 1114–1118.

Sasaki, K., Tamura, S., Tachibana, H., Sugita, M., Gao, Y., Furuyama, J., Kakishita, E., Sakai, T., Tamaoki, T., Hashimoto-Tamaoki, T., 2000. Expression and role of p27(kip1) in neuronal differentiation of embryonal carcinoma cells. Brain Res. Mol. Brain Res. 77, 209–221.

Shou, J., Zheng, J.L., Gao, W.Q., 2003. Robust generation of new hair cells in the mature mammalian inner ear by adenoviral expression of Hath1. Mol. Cell. Neurosci. 23, 169–179.

Tarui, T., Takahashi, T., Nowakowski, R.S., Hayes, N.L., Bhide, P.G., Caviness, V.S., 2005. Overexpression of p27Kip1, Probability of Cell Cycle Exit, and Laminar Destination of Neocortical Neurons. Cereb. Cortex. 15, 1343–1355.

Woods, C., Montcouquiol, M., Kelley, M.W., 2004. Math1 regulates development of the sensory epithelium in the mammalian cochlea. Nat. Neurosci. 7, 1310–1318.

ELSEVIER

Bone 39 (2006) 414–419

BONE

www.elsevier.com/locate/bone

Rapid Communication

Resorption of auditory ossicles and hearing loss in mice lacking osteoprotegerin

Sho Kanzaki [a], Masako Ito [c], Yasunari Takada [b], Kaoru Ogawa [a], Koichi Matsuo [b,*]

[a] *Department of Otolaryngology, School of Medicine, Keio University, 35 Shinanomachi, Shinjuku-ku, Tokyo 160-8582, Japan*
[b] *Department of Microbiology and Immunology, School of Medicine, Keio University, 35 Shinanomachi, Shinjuku-ku, Tokyo 160-8582, Japan*
[c] *Department of Radiology, Nagasaki University School of Medicine, 1-7-1 Sakamoto, 852-8501 Nagasaki, Japan*

Received 15 September 2005; revised 16 January 2006; accepted 31 January 2006
Available online 24 March 2006

Abstract

Bones conduct sound in the middle ear. The three ossicles—the malleus, incus, and stapes—form a chain that transmits vibrations from the tympanic membrane to the oval window of the inner ear. Little is known about bone remodeling events in these ossicles and about potential effects of osteoporosis on hearing loss. Osteoclastic bone resorption is enhanced in $Opg^{-/-}$ mice lacking osteoprotegerin, which is a soluble decoy receptor for the osteoclastogenic cytokine RANKL. We asked whether auditory ossicles are resorbed in $Opg^{-/-}$ mice, and whether these mice suffer from impaired auditory function. All three ossicles in $Opg^{-/-}$ mice showed thinning, especially at the malleal manubrium and incus body. Most notably, unlike in the case in wild-type mice, the junction between the stapes and the otic capsule was fixed in $Opg^{-/-}$ mice, and the stapedial footplate was thinner and broader. Radiological analyses revealed that malleal cortical thickness was positively correlated with tibial bone mineral density in $Opg^{-/-}$ and control littermate mice. Furthermore, progressive hearing loss was detected in $Opg^{-/-}$ mice starting at 6 to 15 weeks of age. These data suggest that osteoprotegerin plays a crucial role in hearing by protecting the auditory ossicles and otic capsule from osteoclastic bone resorption.

Keywords: Bone remodeling; Osteoclast; Osteoprotegerin; Hearing loss; Auditory ossicles

Introduction

The three ossicles in the middle ear, the malleus, incus, and stapes, are formed mainly by endochondral ossification of the mesenchyme from the first and second branchial arches [1,2]. The manubrium (handle) of the malleus attaches to the tympanic membrane, while the footplate of the stapes attaches to the oval window of the cochlea. The stapedial foot is mobile and transmits vibrations to the perilymph, the fluid in the inner ear. The inner ear is contained in the otic capsule of the temporal bone, which is the hardest bone in the body.

Bone mineral density (BMD) is determined by the balance between bone resorption by osteoclasts and formation by osteoblasts. Genetic studies of osteopetrotic mice reveal a number of molecules essential for osteoclastogenesis. Osteoclasts differentiate from precursors of the monocyte–macrophage lineage in the presence of the two membrane bound cytokines, macrophage-colony stimulating factor (M-CSF) and RANKL (receptor activator of nuclear factor-κB ligand, also called osteoclast differentiation factor or TRANCE) [3]. The RANKL receptor is a tumor necrosis factor receptor superfamily member known as RANK encoded by the *Tnfrsf11A* gene. RANK signaling in osteoclast precursors activates a series of osteoclastogenic transcription factors including NF-κB, c-Fos/AP-1, and NFATc1 [4–9]. The osteoclastogenic activity of RANKL is masked by the soluble decoy receptor osteoprotegerin (OPG, also called osteoclast inhibitory factor), encoded by *Tnfrsf11B* [10,11]. In bone remodeling, BMD is maintained by a coupling of osteoclastic bone resorption with subsequent osteoblastic formation [12].

In human populations, the incidence of osteoporotic hip fracture increases exponentially with age [13]. Age-related hearing loss, or presbycusis, affects more than one third of individuals above the age of 75 [14]. Although a link between osteoporosis and hearing loss has been suggested [15–17],

* Corresponding author. Fax: +81 3 5360 1508.
E-mail address: matsuo@sc.itc.keio.ac.jp (K. Matsuo).

8756-3282/$ - see front matter © 2006 Elsevier Inc. All rights reserved.
doi:10.1016/j.bone.2006.01.155

recent epidemiological studies reveal no correlation of hearing loss and osteoporosis in elderly women [18], a finding that seems counterintuitive given that hearing largely depends on bone.

$Opg^{-/-}$ mice develop osteopenia due to enhanced differentiation of osteoclasts [19–22]. To gain deeper insight into the role of bone remodeling in hearing, we asked if auditory ossicles are susceptible to osteoclastic bone resorption in $Opg^{-/-}$ mice and whether auditory function is impaired.

Materials and methods

Mice

Female $Opg^{-/-}$ and heterozygous control mice on a C57BL6 background were purchased from Clea Japan. All experiments were conducted in accordance with institutional review board-approved protocols.

Morphological analyses

Mouse skulls were fixed in 4% paraformaldehyde. For macroscopic analysis, auditory ossicles were isolated by removing the temporal bone, stained for tartrate-resistant acid phosphatase (TRAP) activity using the Leukocyte Acid Phosphatase Kit (Sigma), and observed using a SMZ1500, stereoscopic zoom microscope configured with the Eclipse 90i digital camera system (Nikon). For histological analysis, skulls were decalcified in 0.5 M EDTA for 1 week, and the temporal bones containing auditory ossicles were trimmed and embedded in paraffin. Frontal sections of 5 μm thickness were stained with hematoxylin–eosin (HE) and for TRAP activity.

Radiographical analyses

Each isolated malleus was embedded in melted 8% gelatin in a segment of a plastic drinking straw. After solidifying the gelatin at 4°C, mallei were scanned using micro-computed tomography (μCT) instrumentation (μCT-40, Scanco Medical AG, Switzerland). Based on two-dimensional data from scanned slices, cortical thickness was calculated by setting the volume of interest (VOI) to the entire malleus. Tibial cortical BMD was measured using a CT scanner (*LaTheta* LCT-100, Aloka, Japan) with isolated bilateral tibiae.

Auditory brain-stem response (ABR) measurement

A needle electrode was subdermally inserted at the vertex along the dorsal midline of the scalp between the external auditory canals. The reference electrode was placed below the pinna of the left ear, and the ground electrode was inserted below the contralateral ear. The sound stimulus consisted of a 1 ms tone burst with a rise–fall time of 0.1 ms. For each stimulus, ABR waveforms were recorded for 12.8 ms at a sampling rate of 40,000 Hz using 50–5000 Hz bandpass filter settings, and waveforms from 256 stimuli at a frequency of 9 Hz were averaged. ABR waveforms were recorded in 5-dB sound pressure level (SPL) intervals down from a maximum amplitude until no waveform could be observed using Scope software of the PowerLab system (PowerLab2/20, AD Instruments, Australia). ABRs were performed on mice aged 6, 10, and 15 weeks at the following frequencies: 2, 4, 12, and 20 kHz. ABRs were measured under anesthesia induced by intraperitoneal injection of 0.01 ml/g body weight of 2.5% avertin. The researcher who measured ABRs was unaware of the identities of the animals.

Statistical analysis

Statistical comparisons were performed using Student's *t* test and analysis of variance, where appropriate.

Results

To examine the morphology of the auditory ossicles in $Opg^{-/-}$ mice, we isolated mallei, incudes, and stapes from the middle ear cavities of 10-week-old $Opg^{-/-}$ mice and from wild-type and heterozygous controls. We observed that the junction between the stapes and the oval window of the cochlea was tighter in $Opg^{-/-}$ mice compared to control mice. Ossicles from $Opg^{-/-}$ and control mice were stained for TRAP activity, which is a marker for osteoclasts and resorption lacunae. Compared to wild-type and heterozygous controls, all three ossicles in $Opg^{-/-}$ mice were more heavily stained for TRAP activity and exhibited thinning, particularly at the malleal manubrium, malleal processus brevis, incus body, and stapedial arch (Fig. 1a). Furthermore, the stapedial footplate was thinner and broader at the periphery in $Opg^{-/-}$ mice (Fig. 1a, Stapes, top view). Such thinner parts of ossicles, especially of the stapes, exhibited intense TRAP staining (Fig. 1a).

To further analyze osteoclasts in the auditory ossicles, histological sections of the temporal bone from wild-type, heterozygous, and $Opg^{-/-}$ mice were stained for TRAP activity. Compared to wild-type and heterozygous controls, TRAP-staining was much stronger in both auditory ossicles and the otic capsule in $Opg^{-/-}$ mice (Fig. 1b and data not shown). We next quantitated the number of TRAP-positive multinucleated cells (MNCs) in wild-type, heterozygous, and $Opg^{-/-}$ mice (Fig. 1c). The number of TRAP-positive MNCs was significantly higher in $Opg^{-/-}$ mice than in controls, suggesting that osteoclastic bone resorption of auditory ossicles is dramatically enhanced in $Opg^{-/-}$ mice.

We also histologically examined the junction between the stapes and the otic capsule in heterozygous and $Opg^{-/-}$ mice. The ligament between the stapedial footplate and otic capsule was intact in heterozygous mice (Fig. 2a), while no ligament was seen in $Opg^{-/-}$ mice, and the junction was replaced with bone tissue fusing the stapes and otic capsule (Fig. 2b).

We next examined the auditory ossicles radiographically. Imaging using μCT of isolated mallei confirmed massive erosion in ossicles of $Opg^{-/-}$ mice, which was not observed in heterozygous mice (Fig. 3a). Based on the μCT images, cortical thickness of mallei was calculated in $Opg^{-/-}$ mice and controls. Malleal cortical thickness observed in $Opg^{-/-}$ mice was significantly lower than that seen in heterozygous controls (Fig. 3b). As expected, tibial cortical BMD of $Opg^{-/-}$ mice was also lower than that seen in heterozygous mice (Fig. 3c). Consistent with the histological data, these

Fig. 1. Excess bone remodeling of auditory ossicles. (a) Biomicroscopic photographs showing auditory ossicles from 10-week-old wild-type (+/+), heterozygous (+/−), and $Opg^{-/-}$ (−/−) mice ($n = 6$ or more for each genotype). Ossicles were stained for TRAP activity (red). Arrowheads indicate the malleal manubrium, incus body, and stapedial footplate. Scale bar, 100 μm. (b) Histological sections of auditory ossicles in the middle ear cavity from 15-week-old $Opg^{-/-}$ mice ($n = 2$ per genotype). HE and TRAP activity staining is shown. TRAP-positive areas in the malleus (M), incus (I), and stapes (S) are indicated by arrowheads, and those in the otic capsule by arrows. tm, tympanic membrane. Scale bar, 100 μm. (c) The number of TRAP-positive MNCs in mallei from wild-type, heterozygous, and $Opg^{-/-}$ mice ($n = 5$ for +/+, $n = 4$ for +/− and −/−). $^{\#}P < 0.001$.

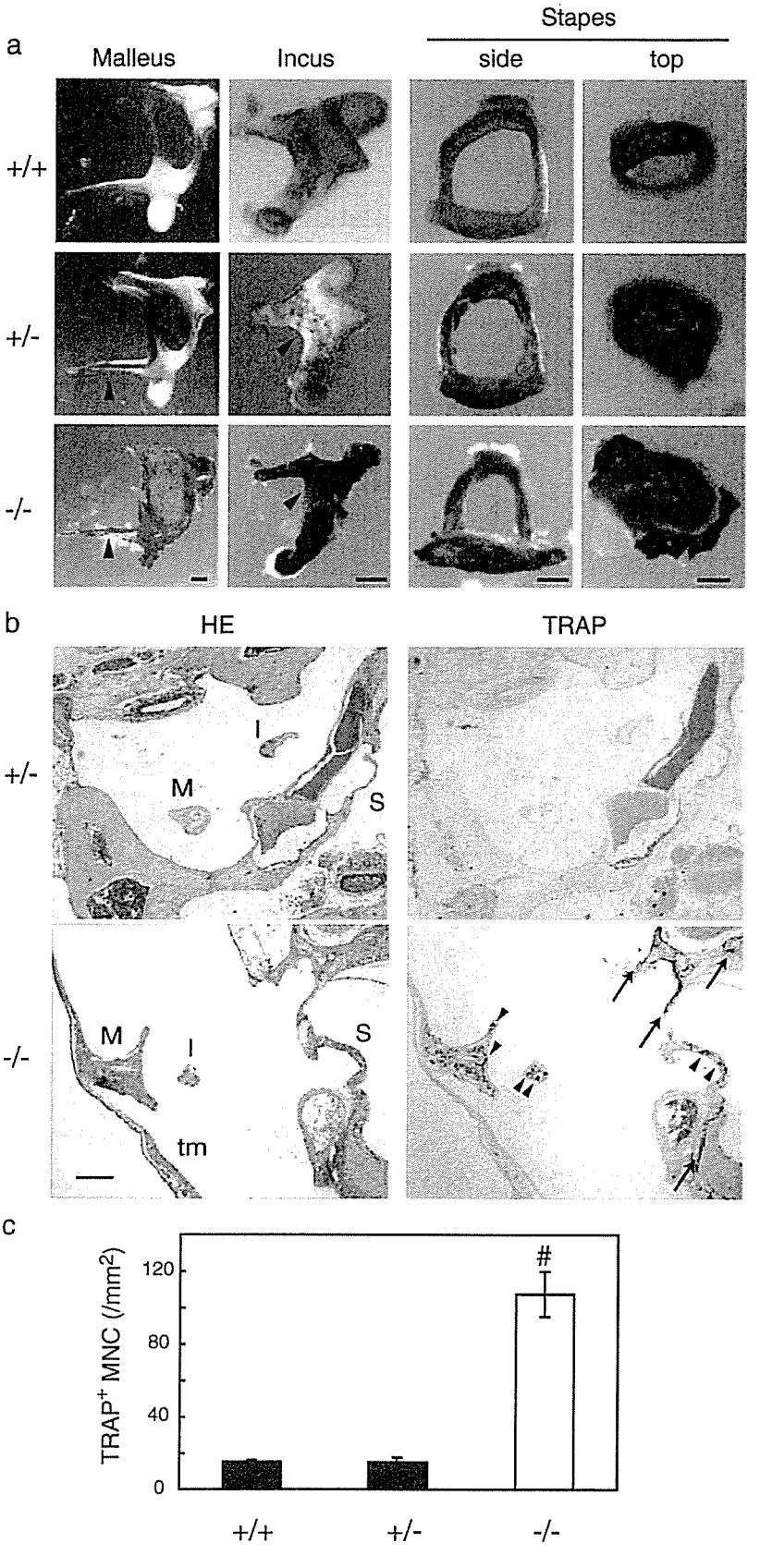
a
Malleus
Incus
Stapes
side
top
+/+
+/-
-/-
b
HE
TRAP
+/-
M
I
S
-/-
M
I
S
tm
c
TRAP+ MNC (/mm2)
120
80
40
0
#
+/+
+/-
-/-

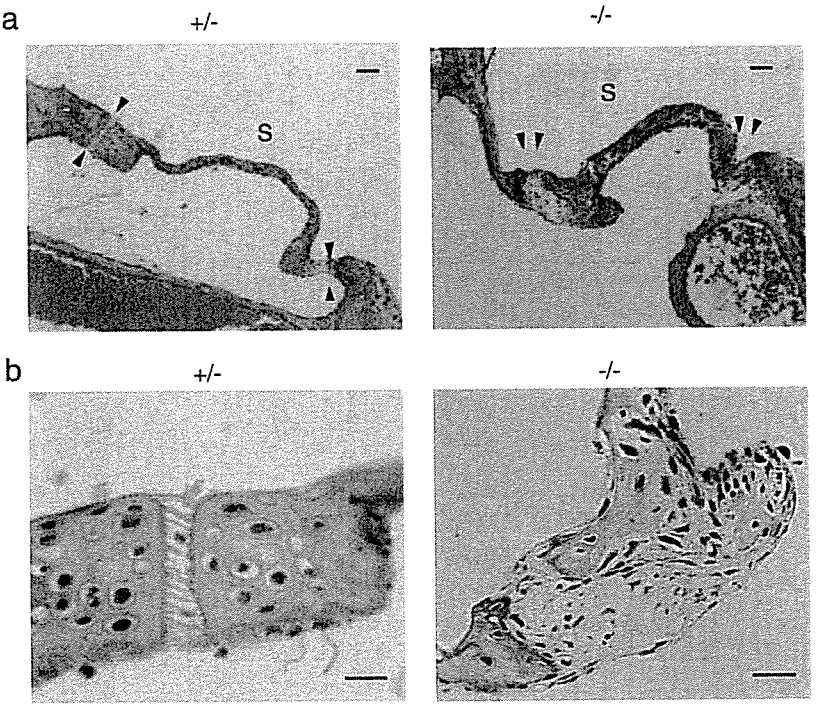

Fig. 2. Histological sections of the stapedial–cochlear junction (arrowheads). Staining is HE (n = 3 for each genotype). Scale bar, 25 μm.

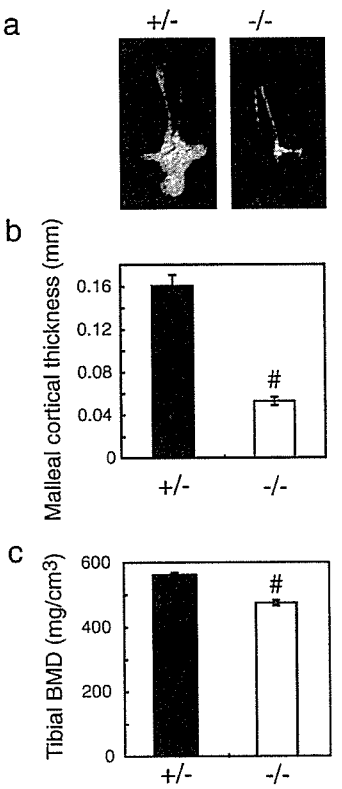

Fig. 3. Radiographical analysis of auditory ossicles and tibia. (a) Representative μCT images of the malleus from 8-week-old mice (n = 5 for +/− and n = 5 for −/−). (b) Malleal cortical thickness of mice described in panel a. (c) Tibial cortical BMD of mice described in panel a. $^{\#}P < 0.001$, versus heterozygous mice.

data suggest that osteoclastic bone resorption of auditory ossicles is elevated in the absence of OPG, leading to bone loss.

To test whether bone loss observed in $Opg^{-/-}$ mice is associated with differences in hearing ability, we assessed ABR thresholds at 6, 10, and 15 weeks of age in heterozygous and $Opg^{-/-}$ mice. ABR threshold was determined as the minimum sound pressure level (SPL) giving reproducible waveforms. At 6 weeks of age, the average ABR threshold of $Opg^{-/-}$ mice was similar to that of heterozygous littermate controls at frequencies from 2 to 20 kHz. However, at 10 weeks of age, $Opg^{-/-}$ mice began showing higher (i.e., worse) thresholds than controls (Fig. 4). By 15 weeks, the differences were even greater, with $Opg^{-/-}$ mice being more than 20 decibels (dB) less sensitive than heterozygous controls at the highest frequency of 20 kHz (Fig. 4). These data suggest that excessive bone remodeling can result in progressive hearing loss.

Discussion

In adult $Opg^{-/-}$ mice, we observed erosion of the malleus, incus, and stapes. Furthermore, TRAP activity was detected in all the three ossicles and the otic capsule of $Opg^{-/-}$ mice, indicating that osteoclastic bone resorption of auditory ossicles is elevated. It is unclear whether certain specific areas within each ossicle are preferentially resorbed or not. We also observed that $Opg^{-/-}$ mice show progressive hearing loss. The precise mechanisms of hearing loss in these mice are currently unknown. Since hearing loss in each animal was progressive, sudden loss of articulation between auditory ossicles is not likely to be the cause of impairment. We observed extensive resorption

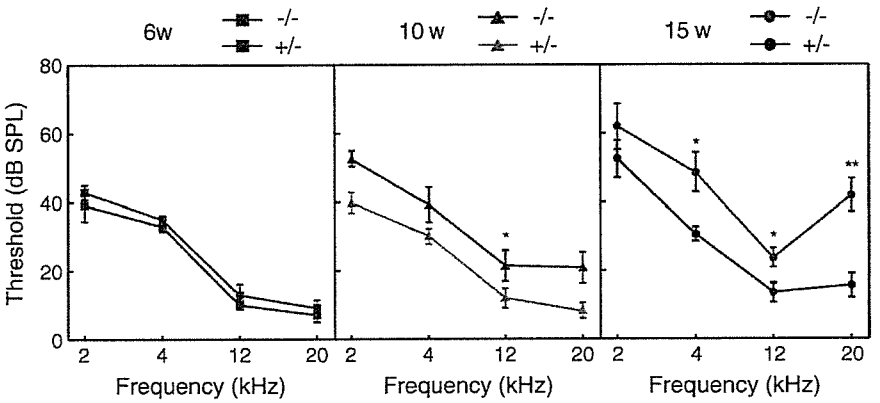

Fig. 4. Progressive increase in ABR thresholds of $Opg^{-/-}$ mice. Data points for thresholds at 2, 4, 12, and 20 kHz in $Opg^{-/-}$ mice and heterozygous controls at the ages of 6 ($n = 5$ each), 10 ($n = 7$ each), and 15 ($n = 7$ each) weeks. Significant differences between 15-week-old $Opg^{-/-}$ and heterozygous control mice are indicated with asterisks ($^{*}P < 0.05$, $^{**}P < 0.01$).

of the malleal processus brevis in $Opg^{-/-}$ mice, but the malleal processus brevis is dispensable for hearing function [2]. In $Opg^{-/-}$ mice, we observed that stapedial fixation, namely, the ligaments between the stapes and the otic capsule, was replaced with bone tissue. Among the observed morphological alterations including thinning of the malleal manubrium and incus body, stapedial fixation is the most likely cause of hearing loss in $Opg^{-/-}$ mice. Clinically, hearing loss in otosclerosis can be cured by surgical intervention at the stapedial–cochlear junction, indicating the importance of this junction in hearing.

OPG deficiency has been found in patients with juvenile Paget's disease, which is also known as idiopathic hyperphosphatasia [23–27] and characterized by markedly increased bone turnover. Paget disease of bone is a distinct and much more common disease than juvenile Paget's disease, characterized by excessive osteoclastic bone resorption followed by compensatory increase in osteoblastic bone formation [28]. Curiously, hearing is affected in approximately 50% of cases of Paget disease of bone involving the skull [29]. Hearing loss in patients with otosclerosis and Paget disease of bone could be due to the increased bone formation, which narrows the internal auditory canal and causes nerve atrophy. On the other hand, hearing loss has been positively correlated with loss of bone density in the otic capsule [30, 31]. Similarly, activating mutations in *TNFRSF11A*, which encodes RANK, cause expansile skeletal hyperphosphatasia, which features deafness in infancy or early childhood [32]. Familial expansile osteolysis, which is also caused by mutation in *TNFRSF11A* [33], is also associated with deafness.

Recent reports show that OPG is highly expressed in cochlear soft tissues and secreted into the perilymph and surrounding bone [34]. Furthermore, OPG levels increase with age in women [35–37]. The apparent lack of association between osteoporosis and hearing loss in humans [18] implies that the auditory ossicles and the otic capsule may be protected from osteoclastic bone resorption by OPG even in patients with postmenopausal and age-related osteoporosis. In conclusion, these data reveal a critical role for OPG as an "audioprotegerin" in maintaining quality of bone conduction by protecting auditory ossicles and the otic capsule from bone resorption. Impaired production of OPG in the temporal bone may be a risk factor for hearing loss.

Acknowledgments

We thank Shumpei Niida, Kyoji Ikeda, and Minako Sato for helpful discussions and Neelanjan Ray and Elise Lamar for critical reading of the manuscript. This work is supported by Grant-in-Aid for Young Scientists B (17791198 to SK) and Grant-in-Aid for Scientific Research B (17390420 to KM) from JSPS, and a Keio University Special Grant-in-Aid for Innovative Collaborative Research Projects.

References

[1] Mallo M. Formation of the middle ear: recent progress on the developmental and molecular mechanisms. Dev Biol 2001;231:410–9.
[2] Zhang Z, Zhang X, Avniel WA, Song Y, Jones SM, Jones TA, et al. Malleal processus brevis is dispensable for normal hearing in mice. Dev Dyn 2003;227:69–77.
[3] Teitelbaum SL, Ross FP. Genetic regulation of osteoclast development and function. Nat Rev Genet 2003;4:638–49.
[4] Karsenty G, Wagner EF. Reaching a genetic and molecular understanding of skeletal development. Dev Cell 2002;2:389–406.
[5] Franzoso G, Carlson L, Xing L, Poljak L, Shores EW, Brown KD, et al. Requirement for NF-κB in osteoclast and B-cell development. Genes Dev 1997;11:3482–96.
[6] Grigoriadis AE, Wang ZQ, Cecchini MG, Hofstetter W, Felix R, Fleisch HA, et al. c-Fos: a key regulator of osteoclast-macrophage lineage determination and bone remodeling. Science 1994;266:443–8.
[7] Matsuo K, Owens JM, Tonko M, Elliott C, Chambers TJ, Wagner EF. *Fosl1* is a transcriptional target of c-Fos during osteoclast differentiation. Nat Genet 2000;24:184–7.
[8] Takayanagi H, Kim S, Koga T, Nishina H, Isshiki M, Yoshida H, et al. Induction and activation of the transcription factor NFATc1 (NFAT2) integrate RANKL signaling in terminal differentiation of osteoclasts. Dev Cell 2002;3:889–901.
[9] Matsuo K, Galson DL, Zhao C, Peng L, Laplace C, Wang KZ, et al. Nuclear factor of activated T-cells (NFAT) rescues osteoclastogenesis in precursors lacking c-Fos. J Biol Chem 2004;279:26475–80.
[10] Simonet WS, Lacey DL, Dunstan CR, Kelley M, Chang MS, Luthy R, et al. Osteoprotegerin: a novel secreted protein involved in the regulation of bone density. Cell 1997;89:309–19.

[11] Yasuda H, Shima N, Nakagawa N, Yamaguchi K, Kinosaki M, Mochizuki S, et al. Osteoclast differentiation factor is a ligand for osteoprotegerin/osteoclastogenesis-inhibitory factor and is identical to TRANCE/RANKL. Proc Natl Acad Sci U S A 1998;95:3597–602.
[12] Martin TJ, Sims NA. Osteoclast-derived activity in the coupling of bone formation to resorption. Trends Mol Med 2005;11:76–81.
[13] Cooper C. Epidemiology of osteoporosis. Primer on the Metabolic Bone Diseases and Disorders of Mineral Metabolism. The American Society for Bone and Mineral Research; 2003. p. 307–13.
[14] Adams PF, Benson V. Current estimates from the National Health Interview Survey, 1991. Vital Health Stat 1992;10:1–232.
[15] Henkin RI, Lifschitz MD, Larson AL. Hearing loss in patients with osteoporosis and Paget's disease of bone. Am J Med Sci 1972;263:383–92.
[16] Haboubi NY, Hudson PR. Factors associated with Colles' fracture in the elderly. Gerontology 1991;37:335–8.
[17] Clark K, Sowers MR, Wallace RB, Jannausch ML, Lemke J, Anderson CV. Age-related hearing loss and bone mass in a population of rural women aged 60 to 85 years. Ann Epidemiol 1995;5:8–14.
[18] Helzner EP, Cauley JA, Pratt SR, Wisniewski SR, Talbott EO, Zmuda JM, et al. Hearing sensitivity and bone mineral density in older adults: the Health Aging and Body Composition Study. Osteoporos Int 2005;16:1675–82.
[19] Bucay N, Sarosi I, Dunstan CR, Morony S, Tarpley J, Capparelli C, et al. *Osteoprotegerin*-deficient mice develop early onset osteoporosis and arterial calcification. Genes Dev 1998;12:1260–8.
[20] Mizuno A, Amizuka N, Irie K, Murakami A, Fujise N, Kanno T, et al. Severe osteoporosis in mice lacking osteoclastogenesis inhibitory factor/osteoprotegerin. Biochem Biophys Res Commun 1998;247:610–5.
[21] Amizuka N, Shimomura J, Li M, Seki Y, Oda K, Henderson JE, et al. Defective bone remodelling in osteoprotegerin-deficient mice. J Electron Microsc (Tokyo) 2003;52:503–13.
[22] Nakamura M, Udagawa N, Matsuura S, Mogi M, Nakamura H, Horiuchi H, et al. Osteoprotegerin regulates bone formation through a coupling mechanism with bone resorption. Endocrinology 2003;144:5441–9.
[23] Cundy T, Hegde M, Naot D, Chong B, King A, Wallace R, et al. A mutation in the gene *TNFRSF11B* encoding osteoprotegerin causes an idiopathic hyperphosphatasia phenotype. Hum Mol Genet 2002;11:2119–27.
[24] Whyte MP, Obrecht SE, Finnegan PM, Jones JL, Podgornik MN, McAlister WH, et al. Osteoprotegerin deficiency and juvenile Paget's disease. N Engl J Med 2002;347:175–84.
[25] Chong B, Hegde M, Fawkner M, Simonet S, Cassinelli H, Coker M, et al. Idiopathic hyperphosphatasia and *TNFRSF11B* mutations: relationships between phenotype and genotype. J Bone Miner Res 2003;18:2095–104.
[26] Janssens K, de Vernejoul MC, de Freitas F, Vanhoenacker F, Van Hul W. An intermediate form of juvenile Paget's disease caused by a truncating *TNFRSF11B* mutation. Bone 2005;36:542–8.
[27] Cundy T, Davidson J, Rutland MD, Stewart C, DePaoli AM. Recombinant osteoprotegerin for juvenile Paget's disease. N Engl J Med 2005;353:918–23.
[28] Roodman GD, Windle JJ. Paget disease of bone. J Clin Invest 2005;115:200–8.
[29] Teufert KB, Linthicum Jr F. Paget disease and sensorineural hearing loss associated with spiral ligament degeneration. Otol Neurotol 2005;26:387–91.
[30] Huizing EH, de Groot JA. Densitometry of the cochlear capsule and correlation between bone density loss and bone conduction hearing loss in otosclerosis. Acta Otolaryngol 1987;103:464–8.
[31] Monsell EM. The mechanism of hearing loss in Paget's disease of bone. Laryngoscope 2004;114:598–606.
[32] Whyte MP, Hughes AE. Expansile skeletal hyperphosphatasia is caused by a 15-base pair tandem duplication in *TNFRSF11A* encoding RANK and is allelic to familial expansile osteolysis. J Bone Miner Res 2002;17:26–9.
[33] Hughes AE, Ralston SH, Marken J, Bell C, MacPherson H, Wallace RG, et al. Mutations in *TNFRSF11A*, affecting the signal peptide of RANK, cause familial expansile osteolysis. Nat Genet 2000;24:45–8.
[34] Zehnder AF, Kristiansen AG, Adams JC, Merchant SN, McKenna MJ. Osteoprotegerin in the inner ear may inhibit bone remodeling in the otic capsule. Laryngoscope 2005;115:172–7.
[35] Yano K, Tsuda E, Washida N, Kobayashi F, Goto M, Harada A, et al. Immunological characterization of circulating osteoprotegerin/osteoclastogenesis inhibitory factor: increased serum concentrations in postmenopausal women with osteoporosis. J Bone Miner Res 1999;14:518–27.
[36] Browner WS, Lui LY, Cummings SR. Associations of serum osteoprotegerin levels with diabetes, stroke, bone density, fractures, and mortality in elderly women. J Clin Endocrinol Metab 2001;86:631–7.
[37] Ueland T, Brixen K, Mosekilde L, Mosekilde L, Flyvbjerg A, Bollerslev J. Age-related changes in cortical bone content of insulin-like growth factor binding protein (IGFBP)-3, IGFBP-5, osteoprotegerin, and calcium in postmenopausal osteoporosis: a cross-sectional study. J Clin Endocrinol Metab 2003;88:1014–8.

Original Paper

Audiology & Neurotology

Audiol Neurotol 2007;12:119–126
DOI: 10.1159/000097798

Received: September 19, 2005
Accepted after revision: September 15, 2006
Published online: December 6, 2006

Sendai Virus Vector-Mediated Transgene Expression in the Cochlea in vivo

Sho Kanzaki[a] Akihiro Shiotani[a, b] Makoto Inoue[c] Mamoru Hasegawa[c] Kaoru Ogawa[a]

[a]Department of Otolaryngology, Keio University, Tokyo, [b]Department of Otolaryngology, National Defense Medical College, Tokorozawa, and [c]DNAVEC Corporation, Tsukuba, Japan

Key Words
Sendai virus vector · Gene transfer · Scala tympani · Scala media · Cochlea · Guinea pig

Abstract
We injected a recombinant Sendai virus (SeV) vector into the guinea pig cochlea using two different approaches – the scala media and scala tympani – and investigated which cell types took up the vector. The hearing threshold shift and distribution of transfected cells in animals using the scala media approach were different compared to those using the scala tympani approach. SeV can transfect very different types of cells, including stria vascularis, spiral ganglion neurons, and sensory epithelia of the organ of Corti, and fibrocytes of the scala tympani. Because SeV vectors can potentially deliver stimuli to the cochlea to induce hair cell regeneration, it may be a powerful tool for repairing the organ of Corti.

Introduction

Gene transfer into inner ear organs is an attractive new approach for treating hearing disorders. This technology can also be useful for treating sensorineural hearing loss, such as inherited deafness [Kanzaki et al., 2002a]. Various viral vectors are capable of carrying out gene transfer. Adenoviruses (AVs) are the most commonly used vectors in experimental studies involving hearing disorders [Kanzaki et al., 2002b, c]. In guinea pigs, adeno-associated virus vectors [Di Pasquale et al., 2005; Lalwani et al., 1996] and herpes simplex virus vectors [Geschwind et al., 1996] have been successfully used for gene transfer into the inner ear. In addition, a new generation of AV vectors has been shown to successfully transfect a few sensory epithelial cells in the guinea pig cochlea [Luebke et al., 2001].

Vectors can be injected into the cochlea through two approaches – the scala media and scala tympani. Of the two, the scala tympani approach minimizes cochlear damage, and thus has been preferred for many gene transfer studies [Kanzaki et al., 2002c; Kawamoto et al., 2004; Yagi et al., 1999]. The scala tympani approach is particularly useful when targeting spiral ganglion neurons, because vectors are taken up selectively by scala tympani fibrocytes, which in turn act as carriers for the delivery to the spiral ganglion neurons. AV-glial cell line-derived neurotrophic factor injections into the scala tympani spare hair cells [Yagi et al., 1999] and spiral ganglion cells [Kanzaki et al., 2002c; Yagi et al., 2000], while effectively delivering glial cell line-derived neurotrophic factor to spiral ganglion neurons. On the other hand, the scala media approach is useful when targeting hair cells for regeneration [Kawamoto et al., 2003]. AV vector injections into the scala media result in reporter transgene expression in supporting cells [Ishimoto et al., 2002], indicating that this vector successfully reaches the sensory epithelial cells.

KARGER
Fax +41 61 306 12 34
E-Mail karger@karger.ch
www.karger.com

1420–3030/07/0122–0119$23.50/0

Accessible online at:
www.karger.com/aud

Sho Kanzaki, M.D., Ph.D
35 Shinanomachi, Shinjuku
Tokyo 160-0016 (Japan)
Tel. +81 3 3353 1211, Fax +81 3 3353 1261
E-Mail skan@sc.itc.keio.ac.jp

Injection via the scala media with AV containing *Atoh1*, a mouse homolog of the *Drosophila* gene *atonal*, caused hair cell regeneration by inducing transdifferentiation of supporting cells [Izumikawa et al., 2005]. The drawback with scala media injections is that such injections may produce an excessive volume of the vector in endolymph or may result in mechanical contact.

Although AVs are effective in transferring genes in clinical situations [Verma and Weitzman, 2005], one problem is that the host response to gene therapy vector exposure involves both the innate and adaptive immune systems. The initial innate immune response also plays a significant role in acute toxicity owing to AV vector exposure [Nazir and Metcalf, 2005]. The cytopathic and immunogenic nature of AV, therefore, precludes its use as transgene vectors for treating hearing disorders in humans. Thus, to make this new technology feasible in humans, it is necessary to develop novel viral vectors that are efficiently transported within the middle and inner ear, but do not produce significant cytopathic and immunogenic responses.

One promising viral vector is Sendai virus (SeV), a member of the Paramyxoviridae family. SeV is an enveloped virus that has nonsegmented, negative-sense genomic RNA [Sakai et al., 1999]. Its replication and gene expression is driven by viral RNA polymerase strictly through a cytoplasmic mechanism [Nakanishi et al., 1998]. SeV vectors have been shown to deliver transgenes to respiratory [Inoue et al., 2004; Yonemitsu et al., 2000], vascular [Masaki et al., 2001], and muscle systems [Shiotani et al., 2001] and neurons [Shirakura et al., 2004]. Now SeV is tested in clinical trials for arteriosclerosis of the lower limbs in Japan.

There are three advantages to using SeV vectors for human gene therapy. First, SeV vectors are completely free of genotoxicity [Bitzer et al., 2003; Griesenbach et al., 2005]. SeV vectors replicate and transcribe transgenes only in the cytoplasm, importantly avoiding interaction with host chromosomes. Second, SeV vectors have remarkably high transfection efficiency in many tissues and cell types. Gene transfer to the respiratory airway via SeV vectors, for example, is at least 10-fold greater than that produced via AV vectors, and is 4- to 5-log-fold greater than that produced via cationic liposomes [Yonemitsu et al., 1996]. Finally, there is no evidence that SeV is pathogenic in humans. The SeV vector was designed using a rodent respiratory virus and has long been used for preparing hybridomas. In the retinal sensory system, an SeV vector produced high expression levels in retinal pigment epithelium after a brief vector-cell contact time, while AV did not [Ikeda et al., 2002]. Taken together, these data suggest that SeV might be a useful vector for delivering transgenes to other sensory systems, including the auditory system.

These properties make SeV vectors a prime candidate for the use in gene transfer therapy for treating hearing disorders. The aim of this study, therefore, was to evaluate the transfection efficiency of an SeV vector in the cochlea using two delivery pathways, the scala media and scala tympani.

Materials and Methods

Animals

We used 17 albino guinea pigs (250–350 g). All animal experiments were performed in accordance with the guidelines of the Keio University Committee for the Use and Care of Animals. The Keio University is fully accredited by the Association for Assessment and Accreditation of Laboratory Animal Care International.

Experimental Groups

We assigned animals to one of two groups: group 1 animals received either SeV (n = 6) or sterile artificial endolymph (NaCl 1 mM, KCl 126 mM, $KHCO_3$ 25 mM, $MgCl_2$ 0.025 mM, $CaCl_2$ 0.025 mM and K_2HPO_4 1.4 mM; n = 3) [Ishimoto et al., 2002] injections into the cochlea via the scala media, and group 2 animals received either SeV (n = 5) or perilymph (sterile normal Ringer's solution; n = 3) [Kanzaki et al., 2002b] injections into the cochlea via the scala tympani. SeV transfection efficacy was assessed histochemically. Auditory brain stem responses (ABRs) were measured before SeV injection and 3 days after injection, prior to sacrifice, to assess shifts in hearing threshold.

SeV Vectors

The full-length SeV genome contains the following: 3′-end leader followed by six viral genes – nucleocapsid, phospho, matrix, fusion (F), hemagglutinin-neuraminidase, and large proteins – and a small 5′-end trailer sequence (fig. 1). Since the F protein conveys viral infectivity, we used F gene-deleted SeV vectors (SeV/ΔF) in our experiments. SeV/ΔF do not produce infectious progeny [Li et al., 2000]. We constructed SeV/ΔF carrying green fluorescence protein (GFP-SeV/ΔF) as previously described [Li et al., 2000]. Briefly, GFP cDNA was amplified with a pair of *Not*I-tagged primers that contained the following SeV-specific transcriptional regulatory signal sequences: 5′-ATTGGCCGCCGTACGGCCATGGTGAGCAAGGGCGAGGAG-3′ and 5′-ATTGGCCGCCGTACGATGAACTTTCACCCTAAGTTTTTCTTACTTCGGAGCTTTACTTGTACAGCTCGTCCATGCCG-3′. A GFP-SeV/ΔF cDNA (pGFP-SeV/ΔF) was constructed by introducing the amplified fragment into the *Not*I site of the parental pSeV18+/ΔF. pGFP-SeV/ΔF was transfected into LLC-MK2 cells infected with vaccinia virus vTF7–3, which expresses T7 polymerase [Fuerst et al., 1986]. The T7-driven recombinant GFP-SeV/ΔF RNA genome was encapsulated by nucleocapsid, phospho, and large proteins, which were derived from their re-

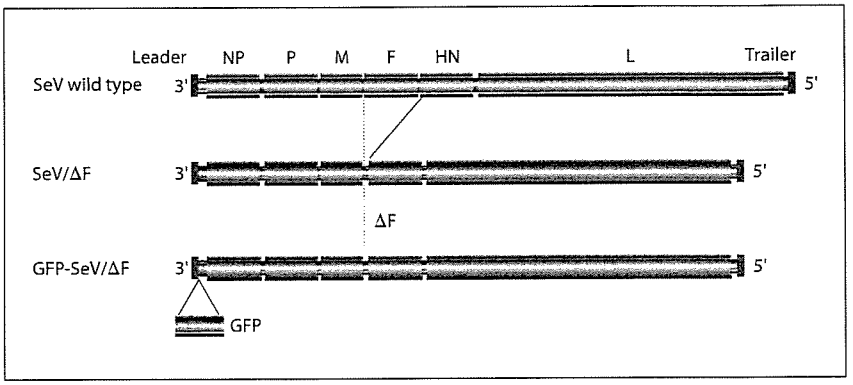

Fig. 1. The structures of the wild type of SeV, SeV/ΔF, and GFP-SeV/ΔF are shown. GFP-SeV/ΔF was used in this experiment. NP = Nucleocapsid; P = phospho; M = matrix; F = fusion; HN = hemagglutinin-neuraminidase; L = large proteins.

spective cotransfected plasmids. The recovered SeV vector was propagated using F protein-expressing packaging cell lines [Li et al., 2000]. Virus titers were determined, and infectivity was expressed as cell infectious units (CIU). The SeV vector was stored at –80°C until use.

Surgery

Guinea pigs were anesthetized with xylazine (10 mg/kg; i.m.) and ketamine HCl (40 mg/kg; i.m.). Prior to vector or control injections, 0.5 ml of 1% lidocaine HCl was injected subcutaneously around the ear as local anesthesia. GFP-SeV/ΔF (titer: 5×10^7 CIU/5 μl) was injected into the cochlea as described below.

In group 1 animals, the ventral side of the left bulla was opened, and a hole was drilled in the lateral wall of the third turn (fig. 2) as previously described [Ishimoto et al., 2002]. In group 2 animals, the left side of the middle ear was exposed via a postauricular approach. Under the guidance of an operating microscope, a small fenestra was made with a sharp probe in the otic capsule at the base of the cochlea [Prieskorn and Miller, 2000; Stover et al., 1999]. To inject SeV, we used a 100-μl Hamilton syringe with an attached vinyl cannula and fine polyamide tip. In group 1 animals, 5 μl of either GFP-SeV/ΔF or endolymph were injected into the scala media, and in group 2 animals, 5 μl of either GFP-SeV/ΔF or perilymph were injected into the scala tympani. Ten minutes after injection, the cannula was removed and the fenestra was covered with a small piece of fascia that adhered to the otic capsule. The bulla defect was sealed with carboxylate cement (Durelon® ESPE America, Norristown, Pa., USA). Dexon® adsorbable suture was used to close the subdermal opening, and nylon suture was used to close the skin opening.

ABR Measurement

A needle electrode was subdermally inserted at the vertex, along the dorsal midline of the scalp between the external auditory canals. The reference electrode was placed below the pinna of the left ear, and the ground electrode was inserted below the contralateral ear. The auditory stimulus consisted of a 1-ms tone burst with a rise-fall time of 0.1 ms. Waveforms from 256 stimuli were delivered at a frequency of 9 Hz. ABR waveforms were recorded for 12.8 ms, sampled at 40000 Hz, bandpass-filtered (50–5000 Hz), and averaged using PowerLab system software (PowerLab2/20, AD Instruments, Castle Hill, Australia). ABR waveforms were recorded in 5-dB SPL intervals from a maximum amplitude until no waveform could be observed. ABRs were recorded at 4, 12, and 16 kHz. The ABRs were measured with the animals under xylazine and ketamine anesthesia (i.m.). The researcher who measured ABRs was blinded to the animal's group assignment.

Statistical Analysis

Unpaired t tests were performed to test for significant differences in ABR thresholds at each frequency between the two groups. SPSS version 13.0 (Chicago, Ill., USA) was used.

Epifluorescent Stereoscopy

Animals were sacrificed under deep anesthesia 3 days after being injected with either vector or control solutions. To perfuse the inner and middle ears locally, we decapitated the animals and removed the temporal bone. The entire cochlea or lateral wall was visualized using a stereoscopic zoom microscope (SMZ1500) configured with epifluorescent optics (Nikon, Tokyo, Japan).

Immunohistochemistry

The cochlea was fixed in 4% paraformaldehyde, decalcified in 10% EDTA, and immersed in sucrose overnight for cryoprotection. After embedding in OCT compound [Whitlon et al., 2001], 10-μm-thick frozen sections were cut and collected. After permeabilization with 0.3% Triton X-100, the organ of Corti was stained for F-actin using a 1:100 solution of rhodamine phalloidin (Molecular Probes, Carlsbad, Calif., USA) for 30 min. The diluent for all solutions was PBS. Whole-mount preparations were observed using an Eclipse 80*i*® digital microscope configured with epifluorescent optics (Nikon).

Results

Transfection of the Cochlea after Injection into the Scala Media

GFP-positive cells were present in the cochlea and middle ear mucosa, including the otic capsule, of the ears receiving vector injections into the scala media

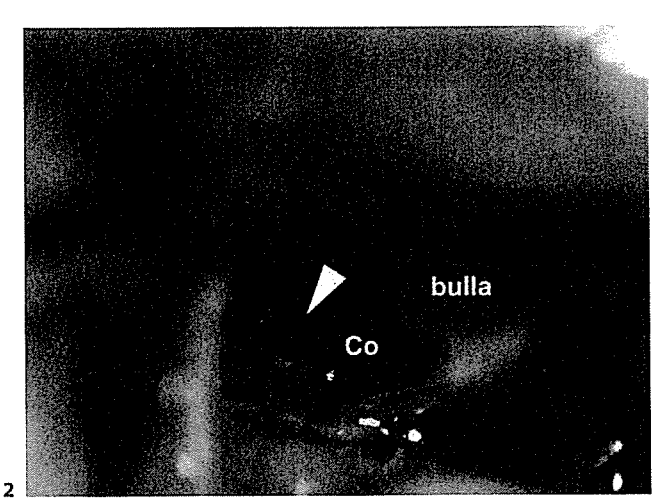

2

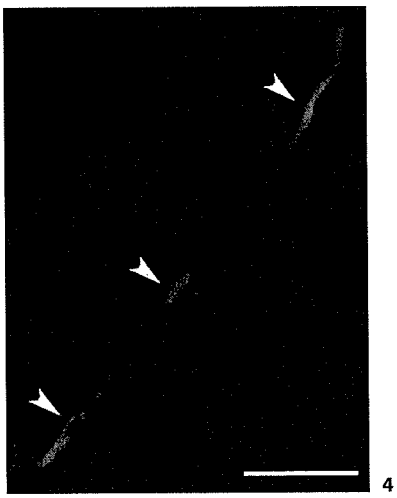

4

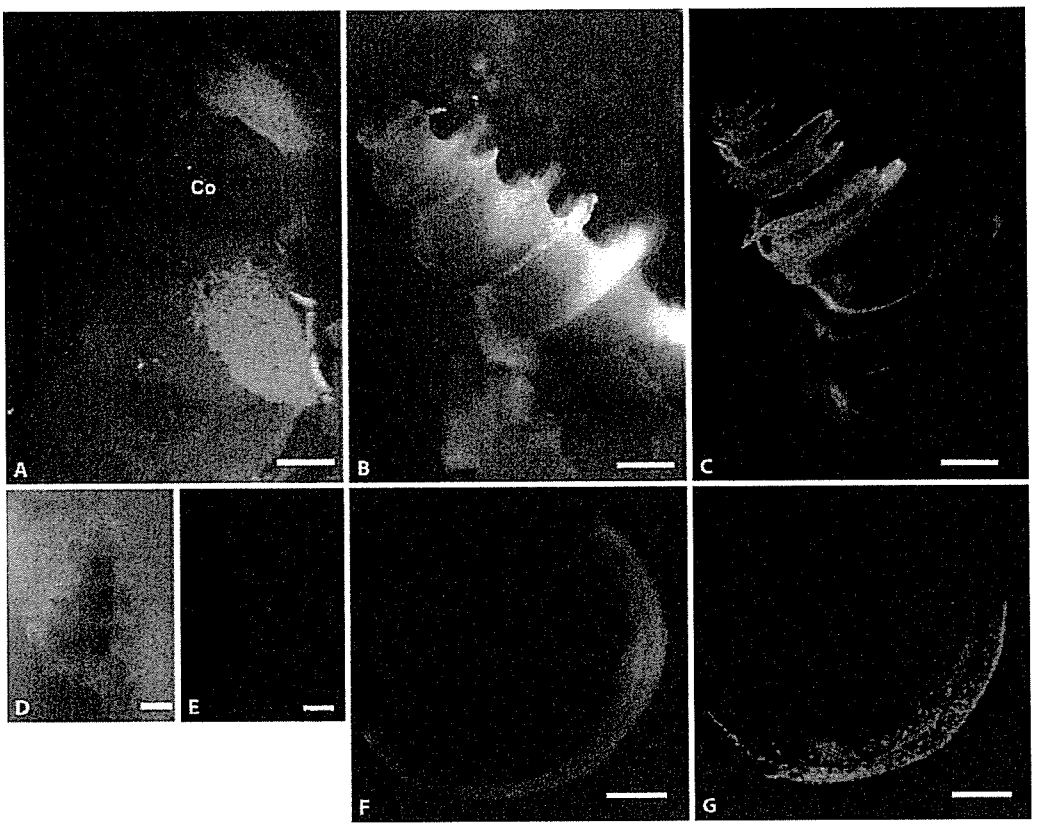

3

Fig. 2. Photomicrograph showing the surgical approach through the scala media. A ventrally located incision was made on the left ear, and then the window of the middle ear bulla was opened. A hole was made in the wall of the cochlear bone (arrowhead). Co = Cochlea; bulla = middle ear bulla.

Fig. 3. Photomicrographs of whole-mounted guinea pig cochlea showing the distribution of GFP-fusion protein after injection of GFP-SeV/ΔF into the scala media. **A** Fluorescent image showing the boney wall of the cochlea. **B**, **C** Light (**B**) and fluorescent (**C**) images of the cochlea of a SeV-inoculated ear. **D**, **E** Light (**D**) and fluorescent (**E**) images of the cochlea in an uninoculated, control ear. **F**, **G** Light (**F**) and fluorescent (**G**) images of the lateral wall of the inoculated ear. Scale bars:1000 μm (**A–E**);600 μm (**F**, **G**).

Fig. 4. Photomicrograph of histological section of guinea pig middle ear after injection of GFP-SeV/ΔF. GFP signal was observed in the middle ear mucosa (arrowheads). Scale bars: 10 μm.

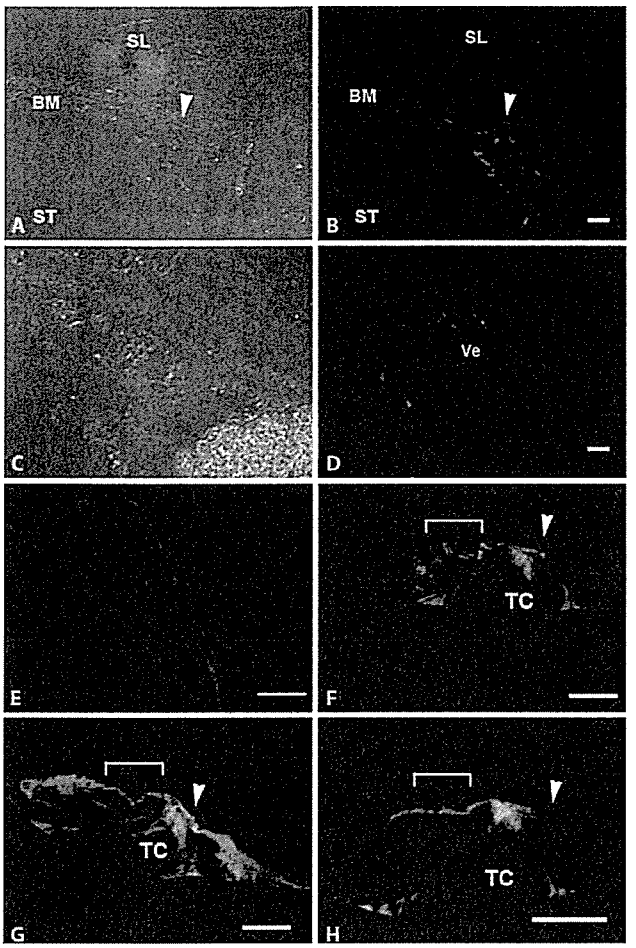

Fig. 5. Photomicrographs of histological sections of guinea pig scala media after injection of GFP-SeV/ΔF. **A**, **B** Spiral ganglion neuron (arrowhead); DIC image (**A**) and fluorescent image (**B**). **C**, **D** Cochlear blood vessel; DIC image (**C**) and fluorescent image (**D**). **E** Stria vascularis. **F–H** Organ of Corti with the arrowhead pointing to the inner hair cell and the bracket suggesting the outer hair cell region; the organ of Corti from an inoculated ear (**F**, **G**) and an uninoculated control ear (**H**). Red = F-actin stained with rhodamine phalloidin; green = GFP-SeV/ΔF-transfected cells; BM = basement membrane; SL = spiral limb; ST = scala tympani; TC = tunnel of Corti; Ve = cochlear blood vessel. Scale bars: 100 μm (**A–D**), 50 μm (**E**), 10 μm (**F–H**).

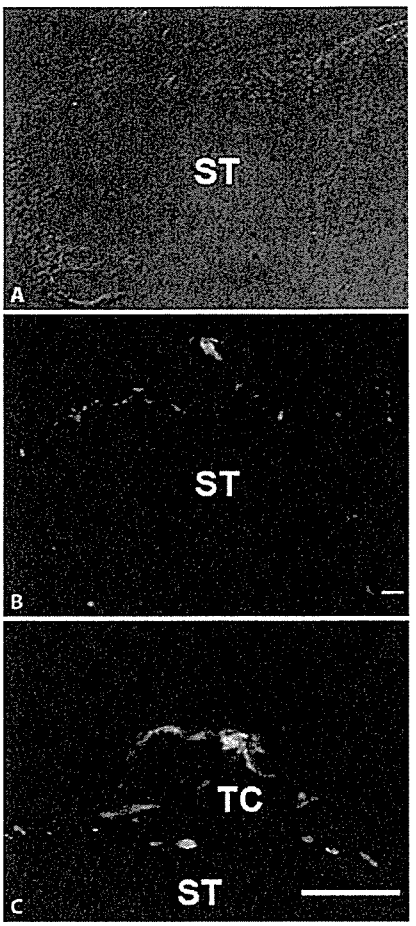

Fig. 6. The cochlea from an ear inoculated with GFP-SeV/ΔF via a scala tympani approach. **A–C** The organ of Corti and fibrocytes of the scala tympani; DIC image (**A**) and fluorescent image (**B**), and higher magnification (**C**); numerous labeled fibrocytes in the scala tympani. ST = Scala tympani; TC = tunnel of Corti. Scale bars: 100 μm (**A**, **B**), 10 μm (**C**).

(fig. 3A–C, fig. 4). This suggests that the injection leaked out of the cochlea and onto the middle ear mucosa. There were no GFP-positive cells in the contralateral ear (fig. 3D, E). GFP was also found in the lateral wall (fig. 3F, G). In one of the inoculated cochlea, GFP localized to several types of cells in several spiral ganglion neurons, in the outer layers of cochlear blood vessels and in the stria vascularis (fig. 5A–E). Transfected cells were found in the outer hair cell layer but not in the inner hair cell layer. In several animals, supporting cells (pillar, Hensen, Deiters, and Claudius cells) and inner and outer sulcus cells were also transfected (fig. 5F, G). We observed no GFP-positive cells in the uninoculated cochlea (fig. 5H).

Transfection of the Cochlea after Injection into the Scala Tympani

GFP-positive signals were found in many fibrocytes in the scala tympani of the inoculated ears (fig. 6A–C) but not in the contralateral or uninoculated ears (control)

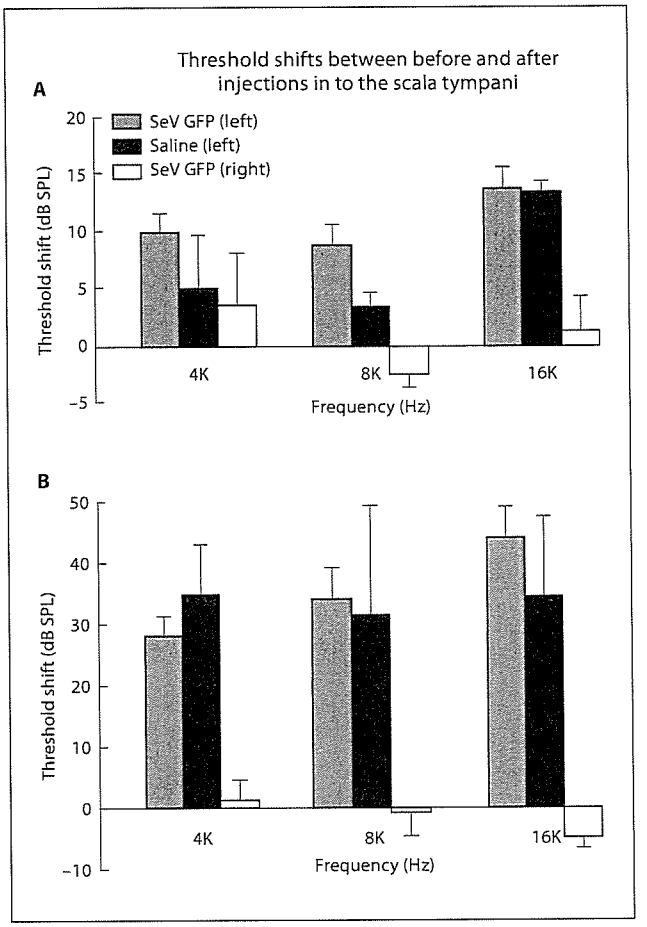

Fig. 7. ABR threshold shifts observed before and after injections via scala media (**A**) and scala tympani (**B**) approaches.

(data not shown). No GFP-positive cells were found in the scala media and vestibuli.

ABR Threshold Shift before and after Vector Injections

Hair cells disappeared in the animals that received SeV injections into the scala media. No obvious damage was seen, however, in the cochlea or middle ear of animals that received injections into the scala tympani. This is consistent with our ABR results, showing that pre- and postinjection threshold shifts were lower in animals operated through the scala tympani approach than in animals operated through the scala media approach. There were no statistically significant differences in hearing threshold shift among the animals that received SeV vector, endolymph, or perilymph injections, indicating that the SeV vector did not affect hearing function.

Table 1. Distribution of transgene expressions after SeV injection via scala media and tympani

Via scala media approach (n = 6)	Animals
Distribution of expression	
All (four) turns	3
Two turns	2
One turn	1
Site of expression	
Scala media	
Stria vascularis	2
Spiral ganglion neurons	1
Vessel	1
Reissner's membrane	1
Organ of Corti	
Inner hair cell	1
Outer hair cell	2
Pillar cells	2
Deiters cells	2
Hensen cells	6
Claudius cells	6
Inner sulcus cells	2
Scala tympani	
Fibrocytes	1
Via scala tympani approach (n = 5)	**Animals**
Distributions of expression	
All (four) turns	1
Two turns	2
One turn	2
Site of expression	
Scala tympani	
Fibrocytes	5

In group 1 (scala media approach), GFP-positive expressions were found at all turns (n = 3 ears), two turns (n = 2), and one turn (n = 1). GFP-positive transfection was found at a wide variety of cells at the scala media and tympani including the organ of Corti. In group 2 (scala tympani approach), GFP-positive expressions were found at all turns (n = 1), two turns (n = 2), and one turn (n = 1). GFP-positive transfection was found at numerous fibrocytes of the scala tympani but not scala media.

Discussion

Distribution of SeV-Transfected Cells

Our findings indicate that SeV vectors (5.0×10^7 CIU/5 μl) can efficiently transfer transgenes to a wide variety of cell types in the organ of Corti, including stria vascularis cells, spiral ganglion neurons (through scala media injections) and fibrocytes (through scala tympani injections) (table 1). The extent of SeV transfection is comparable to that obtained with AV vectors. When AV

vectors are injected into guinea pig cochlea at 1.0×10^{11} virus particles/ml (approximately 5.0×10^{8} virus particles/5 μl) via a scala media approach, AV vectors reach supporting cells such as interdental cells, inner sulcus cells, and Hensen cells [Ishimoto et al., 2002].

SeV may reach the sensory epithelial cells, spiral ganglion neurons, and stria vascularis by traversing the endolymphatic space and the lateral wall of the scala media. The route by which SeV vectors transfect spiral ganglion neurons is unknown. The vectors may penetrate the habenulae perforatae, in which the spiral ganglion nerve runs through a hole in the tympanic lip of the osseous spiral lamina. When injected via the scala tympani approach, SeV cannot penetrate the basement membrane and thus does not reach the organ of Corti as well as does AV.

SeV Does Not Affect Hearing Function

We find no significant differences in the hearing threshold of animals that received SeV, endolymph, or perilymph injections, indicating that SeV does not affect hearing function and that SeV may have lower levels of (cochlear) toxicity than do other viruses [Bitzer et al., 2003; Griesenbach et al., 2005]. We did find, however, that hearing function was differentially affected by the two routes of injection through the scala media and scala tympani. ABRs of animals operated via the scala tympani approach were lower than those of animals operated via the scala media approach. This disparity may be due to mechanical damage to the scala media. When AV is injected into the scala tympani, damage to auditory hair cells is limited [Han et al., 2004], whereas when it is injected into the scala media, numerous outer hair cell are damaged [Ishimoto et al., 2002]. This is consistent with our findings that injections into the scala media are more traumatic than injections into the scala tympani because injection via the scala media made pressure of endolymph followed by the rupture of Reissner's membrane which may mix cochlear fluid including perilymph and endolymph. Mixing fluids change Na^+ and K^+ ion in the inner ear and may not maintain homeostasis. The injection hole was also made in spiral ligament and stria vascularis and the direct flow pressed the organ of Corti through the tectorial membrane. This may be sufficient to damage hair cells.

Our data demonstrated that no GFP-positive expression was seen in the contralateral ear. Previous reports demonstrated that injection of 5 μl of AV vector did not transfect into the contralateral ear both via the scala tympani and media approach [Ishimoto et al., 2002]. However, Stover reported that 25 μl of AV was delivered to the contralateral ear [Ishimoto et al., 2002]. The distribution of transfection may depend on the amount of viral volume.

In conclusion, SeV may be useful for delivering a variety of therapeutic genes to the organ of Corti. Recent studies suggested that supporting cells can be induced to undergo mitosis and differentiate into hair cell phenotypes [Raphael, 1992]. Thus, SeV vectors can be used to promote hair cell regeneration by delivering gene products that induce differentiation of supporting cells to hair cells.

Our data demonstrate that SeV may be a powerful therapeutic tool for sensorineural hearing loss diseases to regenerate hair cells and may prevent spiral ganglion neuron degeneration.

Acknowledgements

We thank all the staff of DNAVEC Corporation, especially A. Tagawa, E. Suzuki and N. Kouno for their excellent technical assistance. This work is supported by grants from the Ministry of Health, Labor, and Welfare in Japan (S.K.).

References

Bitzer M, Armeanu S, Lauer UM, Neubert WJ: Sendai virus vectors as an emerging negative-strand RNA viral vector system. J Gene Med 2003;5:543–553.

Di Pasquale G, Rzadzinska A, Schneider ME, Bossis I, Chiorini JA, Kachar B: A novel bovine virus efficiently transduces inner ear neuroepithelial cells. Mol Ther 2005;11:849–855.

Fuerst TR, Niles EG, Studier FW, Moss B: Eukaryotic transient-expression system based on recombinant vaccinia virus that synthesizes bacteriophage T7 RNA polymerase. Proc Natl Acad Sci USA 1986;83:8122–8126.

Geschwind MD, Hartnick CJ, Liu W, Amat J, Van De Water TR, Federoff HJ: Defective HSV-1 vector expressing BDNF in auditory ganglia elicits neurite outgrowth: model for treatment of neuron loss following cochlear degeneration. Hum Gene Ther 1996;7:173–182.

Griesenbach U, Inoue M, Hasegawa M, Alton EW: Sendai virus for gene therapy and vaccination. Curr Opin Mol Ther 2005;7:346–352.

Han D, Yu Z, Fan E, Liu C, Liu S, Li Y, Liu Z: Morphology of auditory hair cells in guinea pig cochlea after transgene expression. Hear Res 2004;190:25–30.

Ikeda Y, Yonemitsu Y, Sakamoto T, Ishibashi T, Ueno H, Kato A, Nagai Y, Fukumura M, Inomata H, Hasegawa M, Sueishi K: Recombinant Sendai virus-mediated gene transfer into adult rat retinal tissue: efficient gene transfer by brief exposure. Exp Eye Res 2002; 75:39–48.

Inoue M, Tokusumi Y, Ban H, Shirakura M, Kanaya T, Yoshizaki M, Hironaka T, Nagai Y, Iida A, Hasegawa M: Recombinant Sendai virus vectors deleted in both the matrix and the fusion genes: efficient gene transfer with preferable properties. J Gene Med 2004;6: 1069–1081.

Ishimoto S, Kawamoto K, Kanzaki S, Raphael Y: Gene transfer into supporting cells of the organ of Corti. Hear Res 2002;173:187–197.

Izumikawa M, Minoda R, Kawamoto K, Abrashkin KA, Swiderski DL, Dolan DF, Brough DE, Raphael Y: Auditory hair cell replacement and hearing improvement by Atoh1 gene therapy in deaf mammals. Nat Med 2005;11:271–276.

Kanzaki S, Kawamoto K, Oh SH, Stover T, Suzuki M, Ishimoto S, Yagi M, Miller JM, Lomax MI, Raphael Y: From gene identification to gene therapy. Audiol Neurootol 2002a;7: 161–164.

Kanzaki S, Ogawa K, Camper SA, Raphael Y: Transgene expression in neonatal mouse inner ear explants mediated by first and advanced generation adenovirus vectors. Hear Res 2002b;169:112–120.

Kanzaki S, Stover T, Kawamoto K, Prieskorn DM, Altschuler RA, Miller JM, Raphael Y: Glial cell line-derived neurotrophic factor and chronic electrical stimulation prevent VIII cranial nerve degeneration following denervation. J Comp Neurol 2002c;454:350–360.

Kawamoto K, Ishimoto S, Minoda R, Brough DE, Raphael Y: Math1 gene transfer generates new cochlear hair cells in mature guinea pigs in vivo. J Neurosci 2003;23:4395–4400.

Kawamoto K, Sha SH, Minoda R, Izumikawa M, Kuriyama H, Schacht J, Raphael Y: Antioxidant gene therapy can protect hearing and hair cells from ototoxicity. Mol Ther 2004;9: 173–181.

Lalwani AK, Walsh BJ, Reilly PG, Muzyczka N, Mhatre AN: Development of in vivo gene therapy for hearing disorders: introduction of adeno-associated virus into the cochlea of the guinea pig. Gene Ther 1996;3:588–592.

Li HO, Zhu YF, Asakawa M, Kuma H, Hirata T, Ueda Y, Lee YS, Fukumura M, Iida A, Kato A, Nagai Y, Hasegawa M: A cytoplasmic RNA vector derived from nontransmissible Sendai virus with efficient gene transfer and expression. J Virol 2000;74:6564–6569.

Luebke AE, Steiger JD, Hodges BL, Amalfitano A: A modified adenovirus can transfect cochlear hair cells in vivo without compromising cochlear function. Gene Ther 2001;8: 789–794.

Masaki I, Yonemitsu Y, Komori K, Ueno H, Nakashima Y, Nakagawa K, Fukumura M, Kato A, Hasan MK, Nagai Y, Sugimachi K, Hasegawa M, Sueishi K: Recombinant Sendai virus-mediated gene transfer to vasculature: a new class of efficient gene transfer vector to the vascular system. FASEB J 2001;15:1294–1296.

Nakanishi M, Mizuguchia H, Ashihara K, Senda T, Akuta T, Okabe J, Nagoshi E, Masago A, Eguchi A, Suzuki Y, Inokuchi H, Watabe A, Ueda S, Hayakawa T, Mayumi T: Gene transfer vectors based on Sendai virus. J Control Release 1998;54:61–68.

Nazir SA, Metcalf JP: Innate immune response to adenovirus. J Investig Med 2005;53:292–304.

Prieskorn DM, Miller JM: Technical report: chronic and acute intracochlear infusion in rodents. Hear Res 2000;140:212–215.

Raphael Y: Evidence for supporting cell mitosis in response to acoustic trauma in the avian inner ear. J Neurocytol 1992;21:663–671.

Sakai Y, Kiyotani K, Fukumura M, Asakawa M, Kato A, Shioda T, Yoshida T, Tanaka A, Hasegawa M, Nagai Y: Accommodation of foreign genes into the Sendai virus genome: sizes of inserted genes and viral replication. FEBS Lett 1999;456:221–226.

Shiotani A, Fukumura M, Maeda M, Hou X, Inoue M, Kanamori T, Komaba S, Washizawa K, Fujikawa S, Yamamoto T, Kadono C, Watabe K, Fukuda H, Saito K, Sakai Y, Nagai Y, Kanzaki J, Hasegawa M: Skeletal muscle regeneration after insulin-like growth factor I gene transfer by recombinant Sendai virus vector. Gene Ther 2001;8:1043–1050.

Shirakura M, Inoue M, Fujikawa S, Washizawa K, Komaba S, Maeda M, Watabe K, Yoshikawa Y, Hasegawa M: Postischemic administration of Sendai virus vector carrying neurotrophic factor genes prevents delayed neuronal death in gerbils. Gene Ther 2004; 11:784–790.

Stover T, Yagi M, Raphael Y: Cochlear gene transfer: round window versus cochleostomy inoculation. Hear Res 1999;136:124–130.

Verma IM, Weitzman MD: Gene therapy: twenty-first century medicine. Annu Rev Biochem 2005;74:711–738.

Whitlon DS, Szakaly R, Greiner MA: Cryoembedding and sectioning of cochleas for immunocytochemistry and in situ hybridization. Brain Res Brain Res Protoc 2001;6: 159–166.

Yagi M, Kanzaki S, Kawamoto K, Shin B, Shah PP, Magal E, Sheng J, Raphael Y: Spiral ganglion neurons are protected from degeneration by GDNF gene therapy. J Assoc Res Otolaryngol 2000;1:315–325.

Yagi M, Magal E, Sheng Z, Ang KA, Raphael Y: Hair cell protection from aminoglycoside ototoxicity by adenovirus-mediated overexpression of glial cell line-derived neurotrophic factor. Hum Gene Ther 1999;10:813–823.

Yonemitsu Y, Kaneda Y, Morishita R, Nakagawa K, Nakashima Y, Sueishi K: Characterization of in vivo gene transfer into the arterial wall mediated by the Sendai virus (hemagglutinating virus of Japan) liposomes: an effective tool for the in vivo study of arterial diseases. Lab Invest 1996;75:313–323.

Yonemitsu Y, Kitson C, Ferrari S, Farley R, Griesenbach U, Judd D, Steel R, Scheid P, Zhu J, Jeffery PK, Kato A, Hasan MK, Nagai Y, Masaki I, Fukumura M, Hasegawa M, Geddes DM, Alton EW: Efficient gene transfer to airway epithelium using recombinant Sendai virus. Nat Biotechnol 2000;18:970–973.

ELSEVIER

Auris Nasus Larynx 34 (2007) 95–100

AURIS NASUS LARYNX
INTERNATIONAL JOURNAL OF ORL & HNS

www.elsevier.com/locate/anl

Cholesterol granuloma surrounding the endolymphatic sac

Sho Kanzaki [a,b,*], Yasutomo Araki [a], Yasuhide Okamoto [a], Akihiro Kurita [a], Kaoru Ogawa [a]

[a] *Department of Otorhinolaryngology, School of Medicine, Keio University, 35 Shinanomachi, Shinjuku, Tokyo 160-8582, Japan*
[b] *Tokyo Electrical Power Company Hospital, Tokyo, Japan*

Received 18 January 2006; accepted 26 May 2006
Available online 17 August 2006

Abstract

We report a unique case of cholesterol granuloma (CG) surrounding the endolymphatic sac (ES). A 49-year-old man presented with the left side of sensorineural hearing loss, tinnitus, and vertigo. Magnetic resonance and computed tomography imaging revealed a CG surrounding the left ES. The patient initially underwent left transmastoid surgical resection of the tumor. At the time of surgery, brown fluid was aspirated from the tumor, but no other tumors were found. Histopathological examination revealed that the tumor contained cholesterol crystals, confirming the diagnosis of CG. At his 12-month postoperative follow-up, there was no evidence of recurrence. We discuss the radiology, pathology, and surgical removal of CGs surrounding ES.

Keywords: Cholesterol granuloma; Endolymphatic sac; Tumor; Surgery

1. Introduction

Endolymphatic sac (ES) is known as the neuroectodermally derived mucous membrane which lines the vestibular system of inner ear and is involved with resorption and production of endolymph. The tumor located in ES is very rare, but it is considered as endolymphatic sac tumor (ELST) which displays papillary adenoma or adenocarcinoma.

Cholesterol granuloma (CG) is containing fibrous and brownish-yellow fluid composed of globular material, lipids, and crystals [1]. CG is usually occurs in petrous apex or middle ear [1].

We have encountered a rare case of CG surrounding the ES. It was difficult to diagnose the tumor as CG before operation because CG and ELST similarly demonstrated high intensity of T1 weighted MRI findings.

Here, we report the radiological details of this case and describe the surgical approach we used to remove the CG.

2. Case report

A 49-year-old male that complained of left-sided hearing loss, tinnitus, and vertigo for 2 years was examined in Tokyo Electrical Power Company Hospital on January 19, 2004. Review of his history indicated that his symptoms progressively worsened. His previous doctor had initially suspected Meniere's disease and had prescribed a diuretic drug.

Upon our examination, there is normal finding in both sides of the tympanic membrane. Pure tone audiogram revealed a moderate sensorineural hearing loss on the left side (Fig. 1). When the patient shook his head, he exhibited right-directed horizontal and circular or rotary nystagmus, suggesting left side of inner ear damage. He did not display other complications beyond those related to the auditory syndrome.

Magnetic resonance imaging (MRI), performed to exclude cerebral and acoustic neurinoma, but showed an enhanced lesion surrounding the ES (Fig. 2A–C). Computed tomography (CT) was performed to assess mass extension and bone destruction (Fig. 2D).

* Corresponding author. Tel.: +81 3 3353 1211; fax: +81 3 3353 1261.
E-mail address: skan@sc.itc.keio.ac.jp (S. Kanzaki).

0385-8146/$ – see front matter © 2006 Published by Elsevier Ireland Ltd.
doi:10.1016/j.anl.2006.05.016

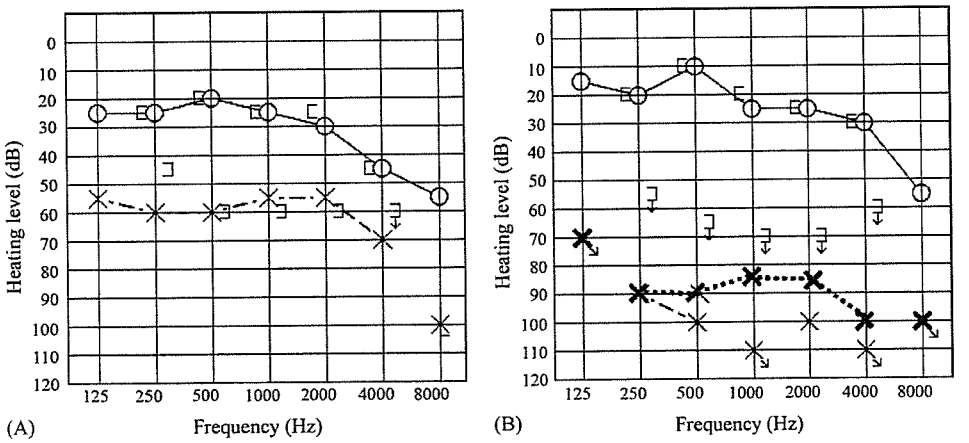

Fig. 1. Pure tone audiogram performed preoperatively (A) and 1 and 6 months postoperatively (B) revealed left-sided hearing loss. Audiograms measured from the left side (air conduction was shown as follows): thin dotted line (1 month), bold dotted line (6 months). The bone conduction has not changed between 1 and 6 month post-operation; Audiogram measured from the right side: solid line.

MRI demonstrated increased signal intensity on T1- and T2- (fluid inversion attenuated recovery; FLAIR) weighted images (Fig. 2A–C). Although these images were highly characteristic of CGs, we did not rule out the possibility of endolymphatic sac tumor (ELST). CT revealed bone destruction around the left ES and enlarged endolymphatic duct (ED) (Fig. 2D) but no compression of the internal auditory meatus. There was no serous effusion in the middle ear cavity. This tumor did not invade the cochlea and semicircular canals. The patient was subsequently moved to the Keio University Hospital for surgery.

After being admitted to the Keio University Hospital, this patient was subjected to several tests, including speech discrimination test, auditory brain stem response (ABR) test, and transient-evoked otoacoustic emission (TEOAE) and distorted product otoacoustic emissions (DPOAE) tests. The speech discrimination test revealed that the patient's speech reception threshold was 95% (60 dB) in the right ear and 65% (90 dB) in the left ear. ABR testing revealed that latency of wave I of the left ear (2.64 ms) was longer than that of the right ear (1.94 ms).

A low wave reproducibility and amplitude reduction were presented in TEOAE and significant response in DPOAE was not presented from the left ear (Fig. 3). Taken together, these audiologic findings suggested cochlear damage. Because symptoms associated with tumor-related compression of the ES are similar to those associated with Meniere's disease [2], we performed a preoperative glycerol test to rule out Meniere's disease. The glycerol test was negative, indicating that the pathologic lesion in this patient was probably not related to typical endolymphatic hydrops or Meniere's disease.

Transmastoid surgery was performed on April 28, 2004. We performed a mastoidectomy with the left side of retroauricular approach while the patient was under general anesthesia. Upon examination, the patient's sigmoid sinus and posterior cranial fossa appeared hypercalcified. Using diamond burs, we removed bone from the posterior fossa at the base of the sigmoid sinus, posteriorly from the sigmoid sinus and anteriorly behind the posterior semicircular canal, to expose bony aspects of the lateral and posterior semicircular canals. To gain access to the tumor, we drilled through the mastoid located behind the posterior semicircular canal. Once exposed, the wall of the CG was opened. Exudates were aspirated (Fig. 4). Following aspiration of the brown (chocolate like) fluid, part of the posterior fossa dura was exposed. We drained the pneumatic space and reestablished adequate aeration of the cavity. The posterior canals, ES, and ED were preserved (Fig. 4). During this time, excised tissue was examined using rapid histology methods and identified as granulation tissue. The mastoid cavity was not obliterated. Immediately after operation, the patient exhibited left-oriented horizontal and circular nystagmus for several hours. Neither meningitis nor facial palsy developed after operation.

Histopathological examination of the excised CG revealed cholesterol crystals, red blood cells and hemosiderin (Fig. 5). Indications of papillary adenoma or carcinoma were not present. The tissue exhibited negative S-100 staining which is a marker of ELST (data not shown). The final diagnosis was CG.

At 2 months after the operation, the left-sided hearing impairment worsened. However, the patient's hearing slightly improved at 6 months after operation. His vertigo disappeared and his hearing continued to improve (Fig. 1B). Caloric testing using 5 ml of 20 °C cold water demonstrated that maximum velocity of the slow phase was 26°/s in left side at 6 months after operation, suggesting that left side of vestibular function was not lost. However, we could not compare the caloric tests between pre- and post-operations because the patient did not want to have this test pre-operation. MRI has revealed no recurrences so far (Fig. 2E).